

299

METEOROLOGICAL OFFICE
London Road, Bracknell, Berks.

METEOROLOGICAL OFFICE
148203
20 MAY 1986
LIBRARY

MET.O.15 INTERNAL REPORT

No 67

Aircraft and dual polarisation radar observations
of hydrometers in light stratiform precipitation

BY

M J Bader, S A Clough and G P Cox

May 1986

Cloud Physics Branch (Met.O.15)

Aircraft and dual polarisation radar observations
of hydrometeors in light stratiform precipitation

by

M J Bader, S A Clough and G P Cox
Meteorological Office, Bracknell

SUMMARY

A case study investigating the relationship of ice phase microphysical structure to differential reflectivity is presented here. The distribution of ice crystal types in light precipitation is discussed and shown to agree with a theoretical model of an individual precipitation fallstreak. The particle characteristics were found to reflect sorting by size and type associated with fall through light wind shear as well as growth in regimes of varying temperature and humidity within the fallstreak.

The observed differential reflectivities were compared with the in-situ particle measurements and the association of high values with planar crystal structures demonstrated. The particle size distribution was found to have a marked influence on radar returns, particularly through the obscuring effects of large particles of indefinite shape. This effect gave rise to relative variations of Z_{DR} which were found to differ from the predictions of monodisperse models. In particular large dendritic crystals of low density were found in this case to be associated with stronger signatures than denser plate-like crystals which from theoretical studies might be expected to produce the greatest differential reflectivity. Because of these complicating factors under stratiform conditions it was concluded that differential reflectivity data must be interpreted with considerable caution in the absence of in-situ measurements or other supporting data.

1. Introduction

The use of radar has been a major element in the development of our present understanding of cloud and precipitation processes in the atmosphere. Dual polarisation radar in particular has been suggested as a means of providing additional information to assist the interpretation of radar reflectivity by reducing uncertainties in the size distribution and physical character of hydrometeors. By measuring the ratio of reflectivity factors for horizontally and vertically polarised radiation (Z_H and Z_V) it is possible to obtain a differential reflectivity Z_{DR} defined by

$$Z_{DR} = 10 \log_{10}(Z_H/Z_V) \quad (1)$$

Z_{DR} is independent of total particle concentration and for collections of identical raindrops is a function of drops size alone. For ice particles however, theoretical studies (eg Dissanayake et al, 1983) have suggested that Z_{DR} should vary appreciably for typically observed particle types, depending upon the particle aspect ratio, refractive index and orientation. Atmospheric observations of Z_{DR} are qualitatively consistent with some of these expectations (Hall et al, 1984), though no comparisons with in-situ

measurements of particle characteristics have yet been reported for the ice phase. The theoretical calculations of Z_{DR} usually refer to the properties of collections of identical particles and the interpretation of observed differential reflectivities remains subject to a number of assumptions about the distribution of particle characteristics. The problem of interpreting variations of Z_{DR} becomes most marked for precipitation including ice particles and near the reflectivity bright band where many ice forms coexist, each with different melting behaviour.

In this work in-situ aircraft particle image sampling has been carried out in light rainfall from stratiform cloud and the results compared with simultaneous colocated dual polarisation radar observations. A wide range of Z_{DR} values was encountered during the experiment, which provides an opportunity to test some of the theoretical predictions and also to demonstrate how observations of differential reflectivity in the ice phase are influenced by microphysical factors. In contrast to most reported studies (eg Stewart et al, 1984) we have attempted to analyse horizontal structure on kilometre scales in order to clarify the underlying microphysical structure, which is discussed in terms of the microphysical evolution of a precipitation fallstreak. This provides a conceptual model in which terminal velocity differences lead to sorting of particles by size and type as they fall through a sheared wind field, an extension of the analysis of Gunn and Marshall (1954). Further, within such a fallstreak, regions of differing microphysical characteristics may be expected as the particle stream falls and is diluted. This model is of value in several ways, providing insight into both the microphysical processes of precipitation growth and the interpretation of the radar observations, especially near the melting layer where particle types are most widely dispersed.

The aircraft microphysical observations are presented in Section 2. In Section 3 the idealised structure of an individual precipitation fallstreak is considered and compared with the microphysical observations. The radar observations are described in Section 4 and the relationships between radar reflectivity, differential reflectivity and the observed hydrometeor distribution are considered. Finally in Section 5 we summarise our results and discuss their implications.

2. In-situ Observations

The data were obtained during an experiment carried out in conjunction with members of the Rutherford and Appleton Laboratory on 15 May 1984. The experimental data consist of dual polarization radar data from the Chilbolton Observatory in Southern England and simultaneous 'in-situ' microphysical measurements obtained from the instrumented C130 Hercules aircraft of the Meteorological Research Flight. During the day the aircraft made a number of horizontal passes through stratiform cloud giving light precipitation; the observations described here were obtained in five of the passes above the melting layer (at 1.3 km height), as detailed in Table 1. Each pass included a 20 km radial track at an air speed of approximately 100 m/s towards the radar, the first four being oriented at an azimuth of 270° and the fifth at 240°, rather later. Navigation accuracy checks and a number of radar observations pinpointing the position of the aircraft to within about 300 m confirm that radar and aircraft data are colocated in space and within 2 minutes of each other in time.

The precipitation encountered was widespread and uniformly light, lasting throughout the 4 hour period of the study. It was located ahead of a slow moving trough, orientated south to north from the Isle of Wight to North-West England. The most important environmental factors in the analysis are the wind shear, which determines the spatial scale of the precipitation sorting process, and the height of the cloud top, about 6.5 km. Wind information was available both from the nearby Larkhill radiosonde ascent at 1100 GMT and the aircraft observations. Due to local variations associated with the development and movement of the trough it is not however possible to define a precise wind profile throughout the observational period. Both sources however indicate that the winds between 1 and 6 km height were predominantly east south easterly (7 m/s maximum), with a positive shear of approximately 1 m/s/km resolved along the 270° azimuth.

a) Aircraft Instrumentation and Data Analysis

The C-130 aircraft is instrumented for a range of meteorological and microphysical studies (Readings (1985)). The aircraft observations used in this work consist of dry bulb temperatures, liquid water content from a Johnson-Williams instrument and particle images from Knollenberg 2D cloud and precipitation probes (Knollenberg, 1970). The cloud probe samples particles passing across a 0.8 mm detector array oriented at right angles to the flight-track with nominal resolution of 25 μm , while the precipitation probe has a 6.4 mm array with resolution 200 μm . The former probe has an approximate sampling volume of 0.1 m³ per kilometre flown and the latter a sampling volume of 1.6 m³ per kilometre, depending slightly upon particle size.

The 2D data and subsequent analysis provide 2-dimensional projected images, derived spectra and estimates of bulk parameters such as rainfall rate and total particle concentrations. Automatically derived bulk parameters and subjective counts of particles are both used in this study, the latter on the basis of a simple classification scheme (crystals are illustrated in Figure 4). The estimation of bulk parameters is dependent upon several assumptions concerning the physical form and density of the imaged hydrometeors. The empirical scheme of Cunningham (1978) was used to estimate the diameter of a water droplet melted from a particular type of crystal. Particle character for this purpose was obtained subjectively by inspection of records similar to those shown in Figure 4 and assumed constant for all images in a particular sample period of 10 seconds. Automatic particle recognition has not been attempted and would be of limited use in this case where many particles are of intermediate or indeterminate character.

Inspection of the particle size distributions indicates that more than 95% of the radar reflectivity under these conditions arises from hydrometeors of diameter (ie maximum dimension) greater than 0.5 mm. The relative fractions of each crystal type were calculated at points along the runs by taking 5 second samples and identifying cloud probe images larger than the 0.5 mm threshold. The precipitation probe was not used for this task as it cannot in general resolve the structure of single crystals. Precipitation elements exceeding 1.5 mm in diameter were generally less well formed and could not be simply classified, with the exception of

needle aggregates. In order to evaluate the concentrations of crystals of particular habits, the relative fractions obtained were multiplied by the total concentration of particles in the 0.5 mm to 1.5 mm size range (as given by the 2D analysis system using data from both probes). This gives an estimate to within 20% of the concentrations of single crystals of each habit in the size range likely to influence radar reflectivities in these conditions. This procedure was carried out for four of the five runs described and the results are displayed in the following sections.

b) Aircraft Observations

Under the ambient conditions it appears from the radar observations that the bulk of the precipitation occurs as relatively narrow streams or precipitation trails (cf Marshall, 1953). These we refer to as fallstreaks (cf Ludlam, 1980) as they resemble the trails of ice often seen falling from cirrus clouds. Post-flight analysis of the particle image data readily locates maxima in the crystal concentrations and the equivalent rainfall rate (shown in Figure 1 for the four sequential passes) provides a good indication of the position of the leading edge of the precipitation fallstreaks. In this section we describe particle size and type distributions in preparation for subsequent discussion of microphysical structure and comparison with the radar observations. The total concentration of large, medium and small elements along the runs is illustrated in Figure 2 while Figure 3 shows the distribution of crystal habits from the subjective analysis. The noisy nature of the data presented in Figure 3 results partly from the small samples used (≈ 70 crystals in a 5 second sample) and likely errors in particle recognition, though the radar observations (Figure 7) also show much variation on small scales. At the highest level (3.7 km, -11.5°C), plateforms dominate the precipitation; there are fewer small dendrites or narrow branched plates, thus it appears that water saturation is barely maintained in the higher part of the cloud (Magono and Lee, 1966); the Johnson-Williams observations are consistent with this hypothesis since measured liquid water contents are low, being less than 0.1 gm^{-3} at all levels from 2.5 km (-4°C) upwards. Capped columns (see Figure 4a for illustration) are distributed almost uniformly at 3.7 km height and account for much of the precipitation outside the fallstreak. At this height the particle images suggest that we can assume that the majority of hydrometeors larger than 1.5 mm are either mixed or irregular growth forms or small aggregates.

Figure 2b illustrates how the size of crystals varies across the fallstreak at a height of 3.1 km (-8°C). The distribution of particle sizes shows a distinct skew (Figures 2b, 3b), also suggested by the radar observations for the same level. The total numbers of crystals in each size class along the length of both upper runs are approximately equal, indicating that no significant growth or aggregation is occurring in the intervening layer (the wind observations suggest that the same trail is seen at both upper levels though different precipitation trails were observed at the lower levels).

At 2.5 km (-4°C) the distribution of hydrometeor sizes and types are shown in Figures 2c and 3c respectively. Concentrations of crystals are extremely high, overloading the 2D probes with 2×10^5 particles per cubic metre at 36 km range. As in many previous observations (eg Heymsfield, 1977) the number of small crystals far exceeds the probable number of

ambient active ice nuclei (Fletcher, 1962). This suggests the operation of an ice multiplication process though the conditions do not seem appropriate for the Hallett-Mossop (1974) process to operate; Johnson-Williams liquid water contents are less than 0.1 gm^{-3} and graupel-like particles are neither likely nor evident. Needles, the typical growth form at this temperature, are locally present in large numbers (Figures 3c, 4c), with a distinct region of needle clumps in the tail of the fallstreak.

Two main fallstreaks were evident at the lowest level (1.9 km, -2°C) one at 36 km and one at 48 km (Figure 2d). Note that in the fallstreak centred at 36 km the largest hydrometeors fall downshear (downshear is downwind in positive shear) of the smaller ones. Aggregates of greater than 2 mm diameter are concentrated primarily between 36 and 39 km, in the leading edge and centre of the fallstreak whereas crystals between 0.2 mm and 0.5 mm are found mainly between 34 and 36 km, in the rear of the fallstreak. The analysis of crystal habits along the run (Figure 3d) indicates two main regions of plateform crystals which constitute the bulk of the two fallstreaks between 34 km and 40 km and also around 48 km. Note that a patch of needles follows the plateforms in both cases (at 32 km and 41 km), while the dendrite concentrations reach their highest values between the regions of plates and needles. Capped columns are few in number and are distributed fairly uniformly along the run both within and outside the fallstreak (Figure 3d). The images indicate that riming is heavy at this level (see Figure 4d) and Johnson Williams data indicate liquid water contents of up to 0.4 g/m^3 .

In summary therefore it appears that the bulk of precipitation is confined to narrow fallstreaks at upper levels which become gradually less distinct lower down. A regular pattern of crystal types and sizes was observed just above the melting layer. In the next section we compare this observed behaviour with the microphysical structure of an idealised fallstreak.

3. Fallstreak structure

The early radar studies of Marshall and co-workers provide a basis for considering the detailed structure of stratiform precipitation which we apply here in the conditions of the experiment. This viewpoint will also prove helpful in interpreting Z and Z_{DR} in the later analysis. Application of the basic geometrical model of Gunn and Marshall (1954) yields the overall shape of a trail while the different parts of the trail provide an environment for particle growth within varying temperature and humidity fields.

Marshall (1953) demonstrated that the characteristic radar patterns of precipitation trails imply that snow is being generated continuously in compact generating elements in the upper levels of stratiform cloud. Ice crystals growing at temperatures around -15°C in such a generating cell will consist of dendrites, plates and sector plates of various types depending upon the supply of water vapour and exact temperature (Magono and Lee, 1966). At higher temperatures different growth characteristics occur, eg columnar growth near -8°C and needle-like growth at around -5°C , while columns, bullets and other dense ice forms are prevalent at lower temperatures.

The following simplified steady state model of a fallstreak is considered: this is based on the conditions seen during the flight. A generating cell exists 3 km above the 0°C isotherm at a temperature of -15°C. If the vertical wind shear is constant and unidirectional then the idealised parabolic trajectories of crystals falling with constant terminal velocity to the melting layer can be determined from the equation (Gunn and Marshall, 1954):-

$$x = \frac{az^2}{2v_T} \quad (2)$$

where a is vertical wind shear per kilometre, x is the relative horizontal displacement of elements from the generating cell, z is the distance fallen and v_T is the terminal velocity of the falling particle. Values of terminal velocity are calculated using the empirical relationships of Heymsfield (1972) and are shown in Figure 5. The wind shear is assumed to be $1 \text{ ms}^{-1} \text{ km}^{-1}$ and, for simplicity, the generating cell is considered as a discrete point. Both dendrites and plateforms may be grown in the vicinity of the generating cell, depending upon the local humidity. If these are allowed to fall freely in the shear described above then their calculated trajectories will be as shown in Figure 6 if no growth occurs. Note that the denser, faster falling plateforms fall closer to the generating cell whereas dendrites are more widely spread. In practice the spatial distribution of dendrites and plates will be less distinct because of the more complex windfield and its variations as well as the multitude of particles with intermediate characteristics. Further, aggregates of plates and dendrites will fall downshear of the majority of single crystals because of their higher fallspeed. Aggregates however are scarce at upper levels since aggregation only becomes efficient at temperatures warmer than -8°C (Pruppacher and Klett, 1978).

The observed distribution of particle types is qualitatively consistent with the predicted behaviour. The effects of sorting by wind shear are most marked in the lowest level (1.9 km, -2°C). In both fallstreaks observed at this level dendrites fall upshear of plateforms, needles fall upshear of dendrites and the distribution of aggregates shows a strong downshear bias (see Figure 2d,3d). Moreover the observed spatial scale of the distribution of crystal habit is consistent with that predicted by the sorting model. With similar weak shear crystals are distributed over about 14 km (Figure 6). Note that a shear of 10 m/s/km would result in a distribution of crystals over 100 km at the melting level, neglecting effects of aggregation. Thus individual packets of precipitation will often overlap, especially in the stronger wind shears typical of frontal systems.

As the particles descend, growth and aggregation is possible depending upon the ambient humidity and temperature. These are functions both of the supply of moisture through ascent and its removal by the growing ice particles (Wexler and Atlas, 1958). Precise observations of humidity and vertical velocity are unfortunately not available for this occasion, though the light precipitation is indicative of weak ascent and riming appears slight except near the melting layer. Even in such light precipitation,

however, estimates of particle diffusion growth rates (see eg Pruppacher and Klett, 1978) from the observed spectra suggest that the competition for moisture would result in only modest supersaturations with respect to ice in the centre of the fallstreak. Nearer the melting layer, where less ascent is necessary to maintain water saturation against diffusion growth, significant liquid water contents of $0.1-0.4 \text{ gm}^{-3}$ are recorded (cf. Wexler and Atlas, 1958).

The observed particle variations strongly suggest the effects of environment upon crystal size and habit. At -8°C most of the particles observed are platelike crystals falling from higher levels apart from a few small columns (0.5 mm) in the centre of the fallstreak, probably symptomatic of weak growth occurring below water saturation at this temperature (Parungo and Weickmann, 1983). At -4°C and -2°C many needles are evident locally and needle clumps are seen in places (see Figures 3,4). The needle crystals occur upshear of the main peaks of platelike crystals, probably because the near-water saturation necessary to sustain needle growth is more readily maintained at this level in regions where the flux of incoming ice particles is not too high. The occurrence of clumps of needles immediately upshear of the main precipitation (Figure 4c) is also consistent with this suggestion. Parungo and Weickmann (1983) suggest that rather than aggregation the growth of needle clumps may occur directly at sites where large droplets impinge upon needles. Figure 6 is presented as a schematic diagram of the structure of a typical fallstreak under the observed conditions. In the following section it will be seen that the separation of precipitation elements through shear sorting leads to distinct patterns in Z and Z_{DR} despite the quantitative limitations of the steady state model.

4. Radar Observations

The relationship of the observed particle distribution to the radar observations is the central topic of this section. Although of secondary interest itself, the radar reflectivity is discussed briefly in order to provide validation of the calculations based on the in-situ observations. The following discussion of differential reflectivity attempts to relate the radar returns qualitatively and quantitatively to the particle characteristics discussed earlier.

a. Radar Reflectivity

The Chilbolton radar has a 25 metre antenna with 0.25° beam width and operating frequency of 3076.5 MHz, the data samples being range-gated to provide 300 m radial average values of Z and Z_{DR} (Hall et al, 1984). Figure 7 shows the radar reflectivity (Z) and the differential reflectivity (Z_{DR}) observed at the time and level of the aircraft passes. All observations within 1.5 beamwidths of the aircraft height are plotted in order to indicate the envelope of Z and Z_{DR} values and their variability. The equivalent radar reflectivity factor Z_e observed by the radar may be defined as:-

$$Z_e = \frac{|K|_i^2}{|K|_w^2} \sum \frac{D_e^6}{V_c} \quad (3)$$

for ice (Smith, 1983). $|K|_i^2$ and $|K|_w^2$ are the dielectric factors for ice and water respectively, while D_e is the equivalent melted diameter and V_c is the illuminated volume. The distribution of largest particles has a marked effect on the observed reflectivity along the runs because of the strong D_e^6 relationship above. Comparison of Figures 2 and 7 demonstrates good agreement between the counts of large particles and reflectivity at all levels. At the upper levels the maximum reflectivity coincides with the leading edge of the precipitation while at 2.5 km it corresponds to the observed area of prolific growth and clumping of needles. As a result of the separation processes discussed in the previous section a much broader reflectivity peak is seen at the lowest levels.

The agreement between radar reflectivity and the concentration of large precipitation elements was tested more quantitatively by applying the empirical relation of Sekhon and Srivastava (1970) for snow:-

$$Z = 1780R^{2.21} \quad (4)$$

to the rainfall rates of figure 1, where R is the precipitation rate in mm/hr. Agreement to within 50% of the peak values of Z was obtained. A direct simulation of the observed reflectivity Z was also carried out from the particle spectra at 3.1 km. Spectra of principal axis length against concentration were obtained for 20 second periods of 2D image data and the equivalent melted diameter computed using Cunningham's (1978) relation

$$D_e = 0.4 D^{0.78} \quad (5)$$

for small snow particles. Knowing the melted diameter, Z was estimated from the spectra using equation 3. The results (shown in Figure 8) are in fair agreement with the reflectivity observed by the radar. The prediction of Z is best at 40 km where the greatest contribution to the reflectivity comes from the largest elements. The general deficit between the predicted and observed reflectivity might be due to undercounting of small precipitation elements but is more probably due to an underestimate in the effective density of these elements, an important but poorly known factor in the calculation.

b) Differential Reflectivity

Many natural hydrometeors are markedly non-spherical and therefore can produce non-zero Z_{DR} . From aerodynamic considerations (Cho et al, 1981) it can be shown theoretically that particles with a well defined major axis such as plateforms, columns and needles should tend to fall steadily with that axis horizontal. Optical phenomena in ice clouds (Ludlam, 1980) and observations of rimed plates and columns (Ono, 1969) confirm that this is indeed the case for single crystals, while Magono and Nakamura (1965) demonstrate that large aggregates may also be aligned. Dissanayake et al

(1983) have calculated differential reflectivity for single ice crystals of selected habit. For a dense plate crystal of axial ratio 0.1 lying in the horizontal and viewed from the side, they estimate that values of Z_{DR} should be about 8 dB. Z_{DR} is found to vary roughly in proportion to bulk density because of the change in refractive index. For planar ice crystals of 0.5 g/cm^3 density, predicted Z_{DR} values are around 5 dB, suggesting that sector plates and branched plates will produce somewhat lower Z_{DR} than solid plates while dendrites, with typical bulk density of 0.3 g/cm^3 , should produce about 3 dB. The Z_{DR} calculation for needles with random orientation in the horizontal plane suggest values of about 1.5 dB. Their calculations also indicate that values of Z_{DR} should be insensitive to variations of 20° or more in particle inclination to the radar beam. We anticipate that Z_{DR} should be approximately zero for aggregate particles. This comes about principally because such particles of low bulk density have smaller dielectric constants and hence (from Equations (6) and (7) below) low Z_{DR} , though their larger axial ratio also tends to reduce Z_{DR} .

Regions of significantly high differential reflectivity were observed at two separate stages of the experiment. It is illuminating to consider first the highest values encountered, which were observed at a time later in the flight than the observations discussed so far. To the south west of the radar a patch of particularly high Z_{DR} values ($> 3 \text{ dB}$) was observed at 3 km height (-7°C) between 35 km and 43 km range. The radar RHI-section at the time of this run is shown in Figure 9. The relatively low reflectivity in the high Z_{DR} region suggests that concentrations of hydrometeors were low and that single crystals were probably dominant. The microphysical observations within the region confirm this, showing that the majority of the hydrometeors were single narrow branched planar or dendritic crystals of up to 2 mm in size (Figure 10a). This confirms that observed values of Z_{DR} can approach the values theoretically predicted for aligned monodispersed ice particles (in this case about 3-4 dB). Since this growth-form is characteristic of conditions of high supersaturation with respect to ice, this area of extensive high Z_{DR} values at around -15°C is probably the result of a weak influx of ice crystals from the cloud above and reduced competition for moisture. This view is consistent with the lower cloud top at this location and the absence of falling crystals such as capped columns, which are common elsewhere along the run (Figure 10b). The very pronounced high Z_{DR} values associated with large dendritic crystals in this case were found to contrast strongly with the commonly observed diffuse pattern of intermediate Z_{DR} . The latter is typified by the observations from the runs described in section 2, which we now consider further.

The differential reflectivity from the four earlier runs is presented in Figure 7. At the highest level (3.7 km, -11.5°C) maximum values of Z_{DR} are around 1.2 dB at 50 km range, somewhat upshear of the main peak in Z . Results from the subjective image analysis (Figures 3a, 4a) indicate a peak in the concentration of plateforms between 49 and 55 km. There appears to be some correlation between the fallstreak and higher Z_{DR} values, though maxima in plateform concentrations and Z_{DR} are not exactly coincident. Figure 7b from the run below this (3.1 km, -8°C) shows maxima of 19 dB in Z and 2.0 dB in Z_{DR} separated by 6 km. This is the area of high Z_{DR} in the radar scan shown in Figure 11. Note that the streak of high Z_{DR} lies on the upshear edge of a prominent precipitation trail. This second region of prominent Z_{DR} is considered in more detail below. Z_{DR} rarely exceeds 1 dB

in the runs at -2°C or -4°C (Figure 7c,d). At a height of 1.9 km (-2°C) the lowest Z_{DR} values of about 0.3 dB occur at 37 km where there are most aggregates. Such regions of low Z_{DR} commonly coincide with stronger precipitation near the melting layer.

There are several possible explanations for the high Z_{DR} values at 3.1 km. It is unlikely that such Z_{DR} values could be due to hydrometeors other than planar crystals. Concentrations of columns and capped columns are substantially lower generally (Figure 3b) and in any case lead to quite low Z_{DR} values. Particle images from the areas of high and low Z_{DR} at this height (see Figure 12) indicate that the single crystals at the two locations are not perceptibly different, while few images in either case correspond to idealised models of pristine crystals. There are no evident distinctions in riming or density likely to lead to the variations in Z_{DR} . If there were significant density variations of single crystals through a fallstreak they might be expected to act in the opposite sense, with denser platelike crystals falling downshear (Pruppacher and Klett, 1978, pp 338-9).

The Z_{DR} values at the peak of the distribution of platform crystals (3.1 km height, 40-42 km range) appear to be reduced by the presence of low numbers of large polycrystalline particles which mask out the high Z_{DR} expected of the single platelike crystals. Even in this light precipitation where particles greater than 1.5 mm diameter are present in small numbers, they still dominate the reflectivity factors to horizontally and vertically polarised radiation because of the large D^6 weighting in each term. In comparing particle size spectra in the low and high Z_{DR} regions substantially greater numbers of the larger particles are evident where Z_{DR} is lower. These larger elements are not sufficiently well defined or frequent in the images to enable us to identify them uniquely. These may be aggregates though it is more probable that they are malformed crystals or else of mixed habit, having developed during particle descent through differing growth regimes. Their most important characteristic appears to be a 3 dimensional overall structure of high axial ratio and low bulk density which leads to low Z_{DR} and high Z . Figure 13 shows the radar reflectivity at this level along with calculated values discussed below. At the location of relatively low Z_{DR} near 40 km the 2500 m^{-3} platelike crystals are diluted by 300 particles per cubic metre exceeding 1.5 mm in diameter. In contrast to this, 850 plates per cubic metre produce the region of high Z_{DR} between 33 and 37 km where the concentration of large masking particles is less than 80 m^{-3} .

In an attempt to provide quantitative estimates of the differential reflectivities to be expected in practice we have calculated Z_{DR} for the particle distributions observed at 3.1 km. The calculation was performed using particle size spectra obtained over 2 km intervals, each spectrum being divided into 15 bins of equal width from 0 to 3 mm. Few single crystals exceed 1.2 mm in diameter and it is assumed that all elements less than this limit can be approximated by uniformly aligned ellipsoids with an axial ratio of 0.1 and dielectric constant 2.00 (corresponding to a density of 0.6 g/cm^3). All hydrometeors larger than 1.2 mm are considered to be spherical scatterers, whose density varies as:-

$$\rho = 0.0707D^{-1.1}$$

(from Locatelli and Hobbs, (1979) mass/size relationship of radiating assemblage of unrimed plates). The Debye assumption (Battan, 1973) is then used to predict the dielectric constant of such particles and Z_{DR} calculated using the Gans theory (eg Seliga and Bringi, 1976).

$$Z_H = \int_0^3 V^2 \left| \frac{(\epsilon-1)}{4\pi + (\epsilon-1)(2\pi - P/2)} \right|^2 N(D) dD \quad (6)$$

$$Z_V = \int_0^3 V^2 \left| \frac{(\epsilon-1)}{4\pi + (\epsilon-1)P} \right|^2 N(D) dD \quad (7)$$

where the shape factor P is given by

$$P = \frac{4\pi (1 - \sqrt{(1 - e^2)/e^2}) \arcsin e}{e^2}$$

V = volume of reflecting ellipsoid

e = eccentricity of ellipse

ϵ = dielectric constant.

The integrals Z_H and Z_V were evaluated for each of the spectra and the resulting Z_{DR} estimates are indicated in Figure 13. While this model is crude the values of Z_{DR} predicted in this manner are in reasonable agreement with those observed. More sophisticated calculations do not appear to be justifiable given both the limited sample volume on a 2 km scale and the substantial assumptions required to model the complex ice phase system.

5. Conclusions

The central objective of the work described here has been to provide a framework for the interpretation of dual polarisation radar observations in ice phase stratiform clouds. Only a single set of observations is available and so generalisation, particularly to heavier precipitation, must be approached with caution. The approach adopted here has differed from most published analyses of dual polarisation radar observations in that it is inherently two (or more generally three) dimensional. The particle sorting process in wind shear leads to both kilometre scale horizontal variations and strong vertical gradients associated with rapid changes of population rather than transitions in a single population.

High values of Z_{DR} (3-4 dB) close to cloud top were in one case found to be unambiguously associated with large dendritic crystals without invoking the possibility of sidelobe effects (Johnson, 1984). The particle distribution for such large single crystals can effectively be considered monodisperse, though this assumption was not generally valid. Regions of significantly high differential reflectivity (1-4 dB) were associated qualitatively with the presence of planar crystal forms throughout, ie plates and dendritic (stellar) crystals, even though these are rarely

pristine in form. This is consistent with theoretical expectations for single aligned crystals (Dissanayake et al, 1983). High expected values of Z_{DR} from these aligned elements such as plate crystals were found to be markedly subject to masking by low concentrations of larger elements because of the D^6 dependence of the reflectivity factors. The relative size and hence reflectivity of crystals in an observed volume of precipitation is thus critical to their identification through Z_{DR} . It seems likely for example that the presence of needle and column crystals will generally not be detectable from Z_{DR} given the lower values predicted, as well as the tendency of needles to form clumps (Parungo and Weickmann, 1983) with reduced bulk density and low Z_{DR} . Although many aggregates are non-spherical and fall with uniform orientation (Magono and Nakamura, 1965) expected Z_{DR} values are around zero simply because of their low bulk density and hence refractive index. There does not seem to be a requirement, or indeed justification, to invoke tumbling effects to explain any of the Z_{DR} variations encountered here. For example, a perfectly aligned ellipsoidal aggregate of axial ratio 0.5 and density 0.07 g/cm^3 would have Z_{DR} of only 0.2 dB on the basis of the Gans theory.

As a result of the masking process our observations in the ice phase indicate that the observed radar patterns strongly reflect the hydrometeor size distribution; low Z and high Z_{DR} are characteristic of very light precipitation (narrow particle spectrum) and high Z and low Z_{DR} appear characteristic of heavier precipitation which includes large particles of lower bulk density. It was found that semi-quantitative verification of Z and Z_{DR} was possible from in-situ particle spectra. However, because of the number of assumptions required to model the complex ice phase system, quantitative interpretation of Z_{DR} alone appears to offer little information to improve upon Z - R relations in light precipitation, except perhaps statistically as an indicator of effective ice density. Additional hydrometeor information from other radar parameters (eg the linear depolarisation ratio (L_{DR})) may however improve computational skill. The qualitative information gained from Z and Z_{DR} patterns together, however, does provide valuable guidance in directing and interpreting in-situ aircraft microphysical observations.

A generating cell/fallstreak model was developed and found helpful in the interpretation of both microphysical observations and radar patterns. During its fall the particle stream evolves under the influence of separation and sorting by terminal velocity variations, while elements grow in temperature and humidity fields modified by the ice distribution. The wind shear is critical in determining the scale of the particle separation. The weak shear present in this case ($\approx 1 \text{ m/s/km}$) led to particle dispersion over about 15 km at the melting layer, though in the stronger shears commonly encountered in frontal systems overlapping trails extending over 50 km or more are likely. The occurrence of different crystal habits at the lowest level studied (-2°C) was found to agree well with the distribution predicted from established fallspeeds for the various particle types. This variation in particle characteristics appears likely to influence the character of the bright band observed in both Z and Z_{DR} .

Throughout the fallstreak the influence of temperature and humidity on the growth of crystals is evident. Where the cloud top descended to about -15°C , small numbers of large narrow-branched plates and stellar dendrites were observed together with high Z_{DR} values (3-4 dB). These growthforms

are characteristic of high relative humidity, probably resulting from weak uplift and reduced concentrations of ice crystals competing for moisture. The lower number of 'cold' crystals such as capped columns is consistent with this suggestion. Small plateforms, numerically the most common constituent of the fallstreak at upper levels, appear to be the primary form of growth here in weak ascent and deep cloud. Lower down in the precipitation trail, fresh particle growth was most evident upshear of the main mass of precipitation, probably because severe competition for moisture within the fallstreak inhibited the growth of individual particles.

The fallstreak model clearly gives rise to some elements of the variation seen in Z_{DR} . The position and shape of diffuse Z_{DR} streaks at the upshear edge of ice fallstreaks (rather than the downshear edge in rain (Atlas, 1984)) indicates that shear induced sorting processes are important. High Z_{DR} here is probably associated with relatively low concentrations of slowly falling plateforms which are not obscured by larger reflective elements of lower bulk density. The streaks are not clearly evident lower in the atmosphere, probably because of the progressive increase in masking due to aggregation at higher temperature as well as the overlap of successive fallstreaks. The slowest falling single crystal remnants of earlier fallstreaks tend to form a background of modest Z_{DR} punctuated by streaks of low Z_{DR} associated with aggregates of lower density (cf Atlas, 1984).

Acknowledgements

We are grateful to J W F Goddard and S M Cherry of Rutherford and Appleton Laboratory for their collaboration in the experiment and helpful discussion of the observations. We also thank C B Hynes and A K Macallan for their help in analysing the data.

References

- | | | |
|--|------|--|
| Atlas, D | 1984 | Highlights of the Symposium on the multiple-parameter radar measurements of precipitation: Personal reflections. Radio Science 19 number 1. 238-243. |
| Battan, L J | 1983 | Radar observations of the atmosphere. University of Chicago press, Chicago, II. |
| Cho, H R, Iribarne, J V and Richards, W G | 1981 | On the orientation of ice crystals in a cumulonimbus cloud. J Atmos Sci, 38, 1111-1115. |
| Cunningham, R M | 1978 | Analysis of particle spectral data from optical array (PMS) 1D and 2D sensors. 4th Symp Met Obs and Inst Apr 10-14; Boston, Mass; Amer Met Soc. |
| Dissanayake, A W, Chandra, M and Watson, P A | 1983 | Prediction of differential reflectivity due to various types of ice particles and ice water mixtures. London Institute of Electrical Engineers Internal Conf. Antenna Propagation Conf Publ 219, 12-15 Apr, Norwich. |
| Gunn, K L S and Marshall, J S | 1954 | The effect of wind shear on falling precipitation, J Met, 12, 339-349. |
| Hall, M P M, Goddard, J W F and Cherry, S M | 1984 | Identification of hydrometeors and other targets by dual-polarisation radar. Radio Sci, 19; 132-141. |
| Hallett, J and Mossop, S C | 1974 | Production of secondary ice particles during the riming process. Nature 249, 26-28. |
| Heymsfield, A J | 1972 | Ice crystal terminal velocities. J Atm Sci 29, 1348-1357. |
| Heymsfield, A J | 1977 | Precipitation development in stratiform ice clouds: A microphysical and dynamical study. J Atm Sci 34, 367-381. |
| Johnson, D B | 1984 | The effect of antenna sidelobes on multiple-parameter radar measurements. Journal Atmos and Oceanic Technology 1, 287-290. |
| Knollenberg, R G | 1970 | The optical array: An alternative to scattering or extinction for airborne particle size determination. J Appl Meteor 9, 86-103. |

- | | | |
|--|------|--|
| Locatelli, J D and
Hobbs, P V | 1974 | Fall speeds and masses of solid precipitation particles. J Geophys Res, 79, 2185-2197. |
| Ludlam, F H | 1980 | Clouds and Storms: The behaviour and effect of water in the atmosphere. Pennsylvania State University Press. |
| Magono, C and Lee, C V | 1966 | Meteorological classification of natural snow crystals. J Fac Sci, Hokkaido Univ 2, 321-362. |
| Magono, C and Nakamura | 1965 | Aerodynamic studies of falling snowflakes. J Meteor Soc Japan, 43, 139-147. |
| Marshall, J S | 1953 | Precipitation trajectories and patterns. J Meteor, 10, 25-29. |
| Ono, A | 1969 | The shape and riming properties of ice crystals in natural clouds. J Atm Sci, 26, 138-147. |
| Parungo, F P and
Weickmann, H K | 1983 | Ice crystal growth at $(-8 \pm 2)^{\circ}\text{C}$. J Rech Atmos, 17, 139-156. |
| Pruppacher, H R and
Klett, J D | 1978 | Microphysics of clouds and precipitation. D Reidel. |
| Readings, C J | 1985 | The use of aircraft to study the atmosphere: the Hercules of the Meteorological Research Flight. Met Mag 114, 66-78. |
| Sekhon, R S and
Srivastava, R C | 1970 | Snow size spectra and radar reflectivity. J Atm Sci, 27, 299-307. |
| Seliga, T A and
Bringi, V N | 1976 | Potential use of radar differential reflectivity measurements at orthogonal polarisations for measuring precipitation. J Appl Meteor, 15, 69-76. |
| Smith, P L | 1984 | Equivalent radar reflectivity factors for snow and ice particles. J Clim Appl Meteor, 23, 1258-1260. |
| Stewart, R E, Marwitz, J D
Pace, J C and Carbone, R E | 1984 | Characteristics through the melting layer of stratiform clouds. J Atmos Sci, 41, 3227-3237. |
| Wexler, R and Atlas, D | 1958 | Moisture supply and growth of stratiform precipitation. J Meteor, 15, 531-538. |

Figure 1. Precipitation rates derived from Knollenberg 2D probe data for the four runs described in the text, at heights of (a) 3.7 km, (b) 3.1 km, (c) 2.5 km, (d) 1.9 km.

Figure 2. The distribution of particle sizes along each of the four runs, at heights as in Figure 1. Ranges of maximum diameters are as follows: - - - - 0.2 - 0.5 mm, 0.5-1.5 mm, ——— 1.5-2.5 mm, -.-.-. greater than 2.5 mm.

Figure 3. Distribution of particles by type along each of the four runs, at heights as in Figure 1.

Figure 4. 2D Knollenberg cloud probe images showing typical crystals for the four runs discussed in the text.

Figure 5. The terminal velocity of selected crystals at 700 mb, evaluated from data given in table 3 of Heymsfield (1972).

Figure 6. The idealised structure of a precipitation fallstreak in constant unidirectional shear. Images are presented from corresponding regions in the observations.

Figure 7. Observations of reflectivity and differential reflectivity colocated with the four aircraft runs described above (see Table 1).

Figure 8. Observed values of reflectivity and values calculated from particle spectra at 3.1 km height along 270° azimuth at 1303Z.

Figure 9. RHI scans of (a) Z, (b) Z_{DR} along an azimuth of 250° at 1505Z.

Figure 10. 2D Knollenberg precipitation and cloud probe images along 250° azimuth at 1505Z.

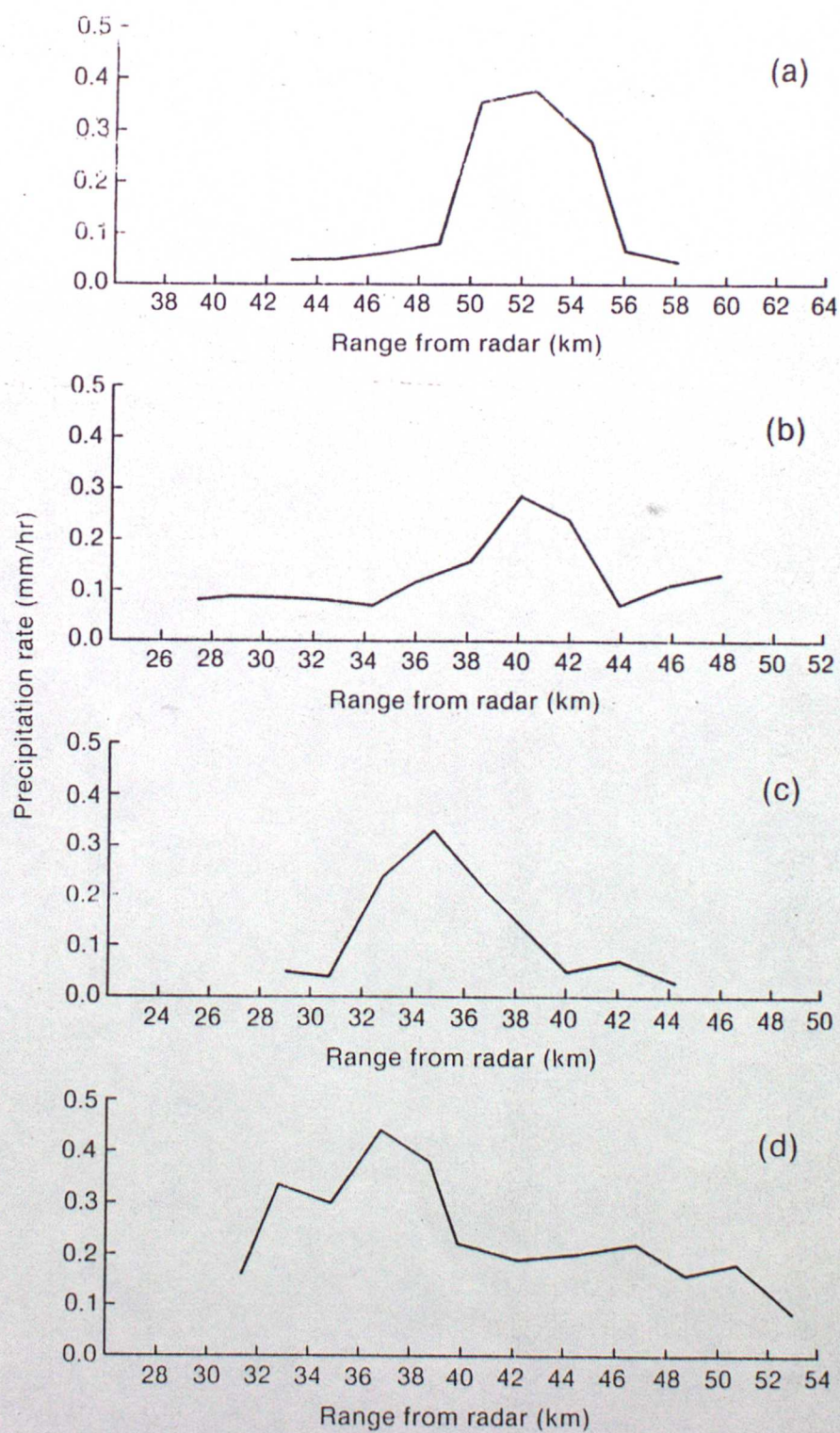
Figure 11. RHI scans of (a) Z, (b) Z_{DR} along 270° azimuth at 1303Z.

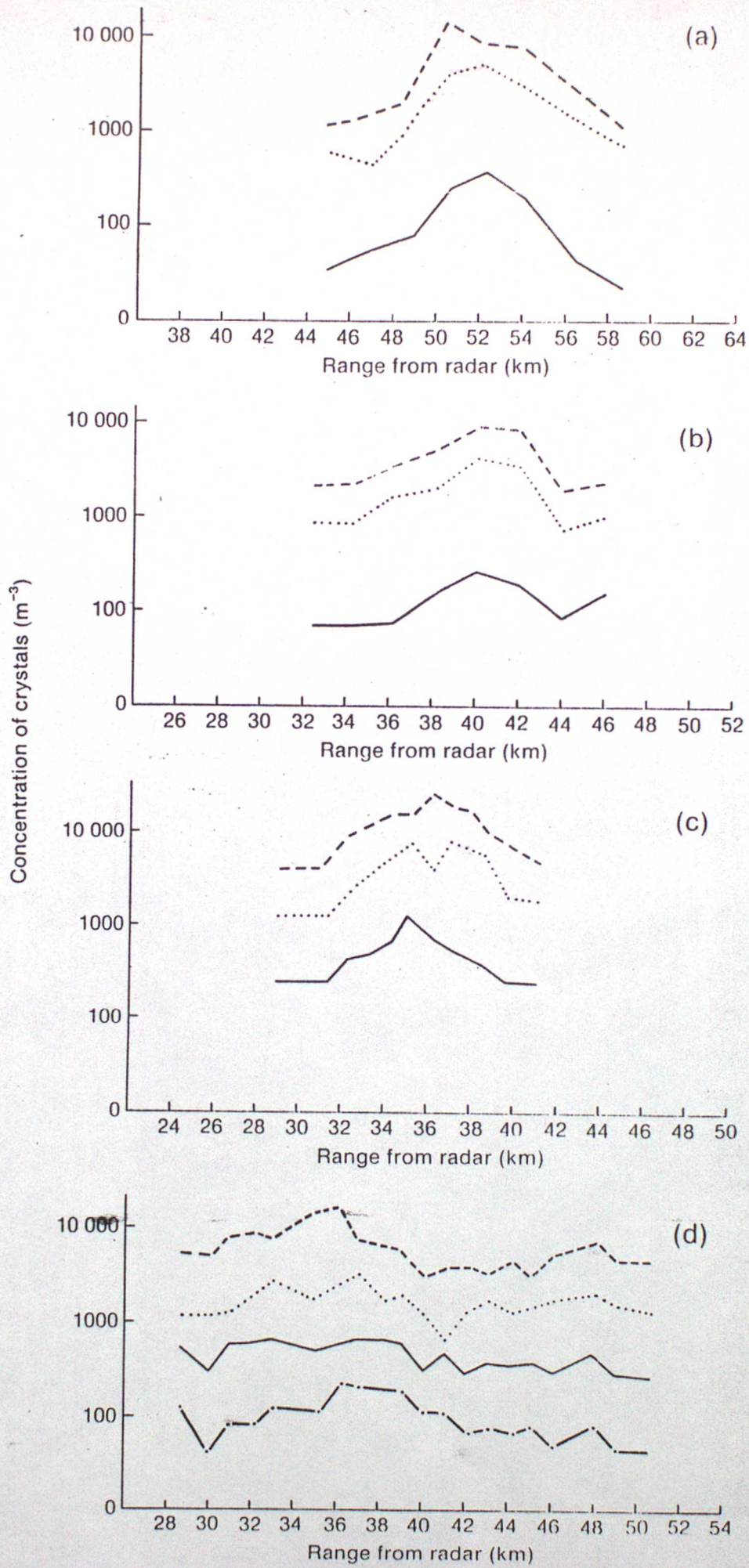
Figure 12. 2D Knollenberg cloud probe images along 270° azimuth at 1303Z.

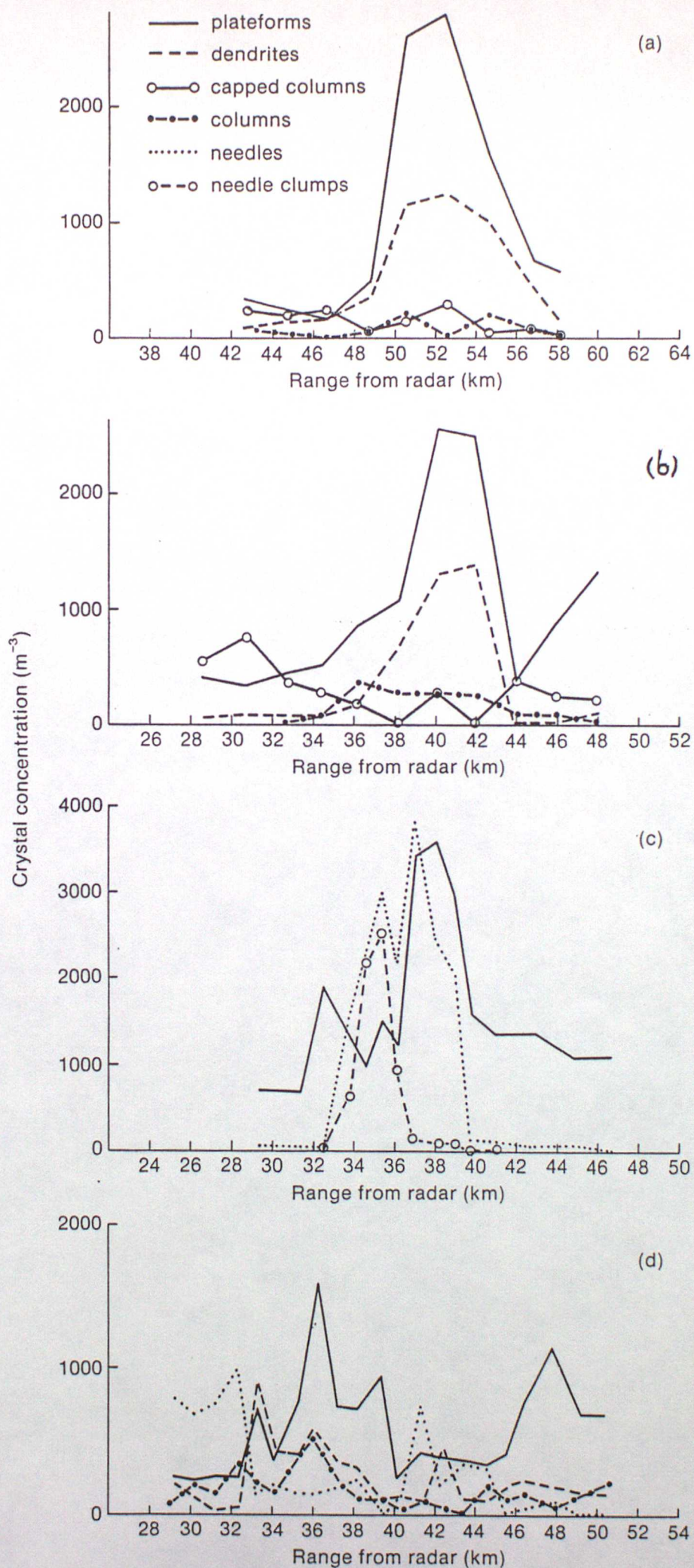
Figure 13. Observed and calculated values of differential reflectivity at 3.1 km along 270° azimuth at 1303Z.

Table 1

<u>Run Height</u>	<u>Average Run Temperature</u>	<u>Approx Time of Run</u>	<u>Range (km)</u>	<u>Azimuth</u>	<u>Observed Hydrometeors</u>
<u>3.7 km</u>	-11.5°C	1318	60-38	270°	Lightly rimed single crystals. Large fractions of capped columns outside fallstreaks.
<u>3.1 km</u>	-8.0°C	1303	50-28	270°	Mixed single crystals.
<u>2.5 km</u>	-4.0°C	1249	50-28	270°	Distinct period of Needles and Needle aggregates, mixed single crystals.
<u>1.9 km</u>	-2.0°C	1234	50-28	270°	Aggregates and heavily rimed single crystals.
-----	-----	-----	-----	-----	-----
<u>3.0 km</u>	-7.0°C	1505	30-50	250°	Dendrites in very light precipitation, capped columns and small plates in heavier precipitation.







(a) Height 3.7 km (-11°C)

Dendrites and sector plates : 53 km



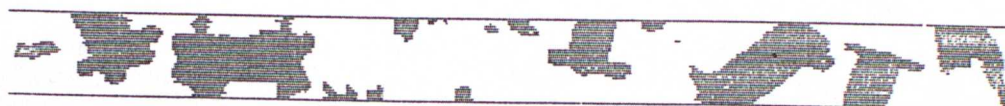
Capped columns : 46 km



0.8 mm

(b) Height 3.1 km (-8°C)

Capped columns : 31 km



Platforms and columns : 37 km

(c) Height 2.5 km (-4°C)

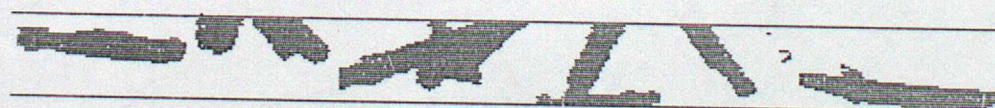
Needles and needle clumps : 33 km



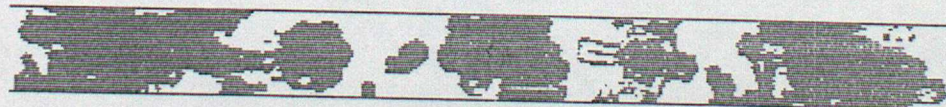
Platforms : 40 km

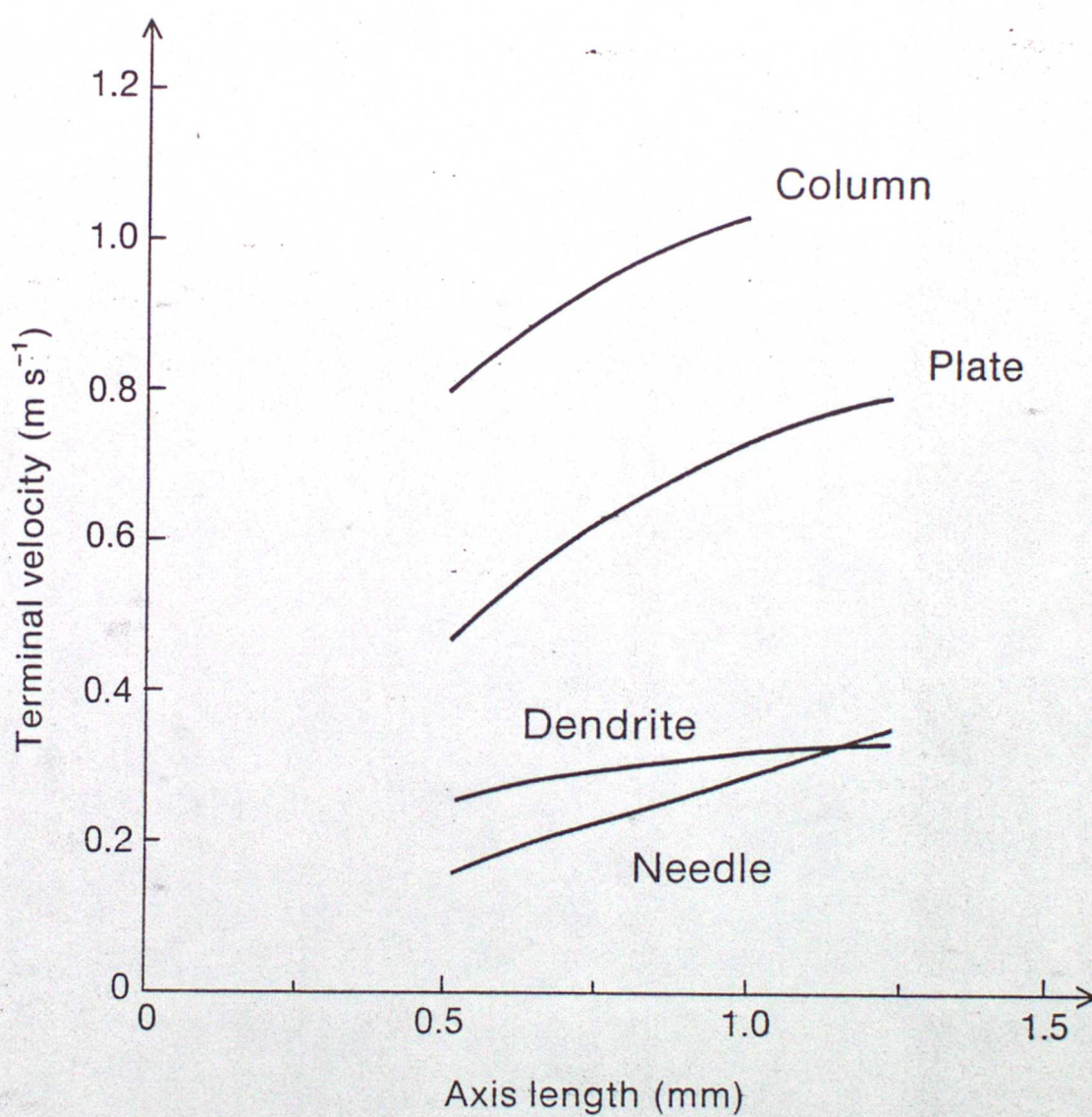
(d) Height 1.9 km (-2°C)

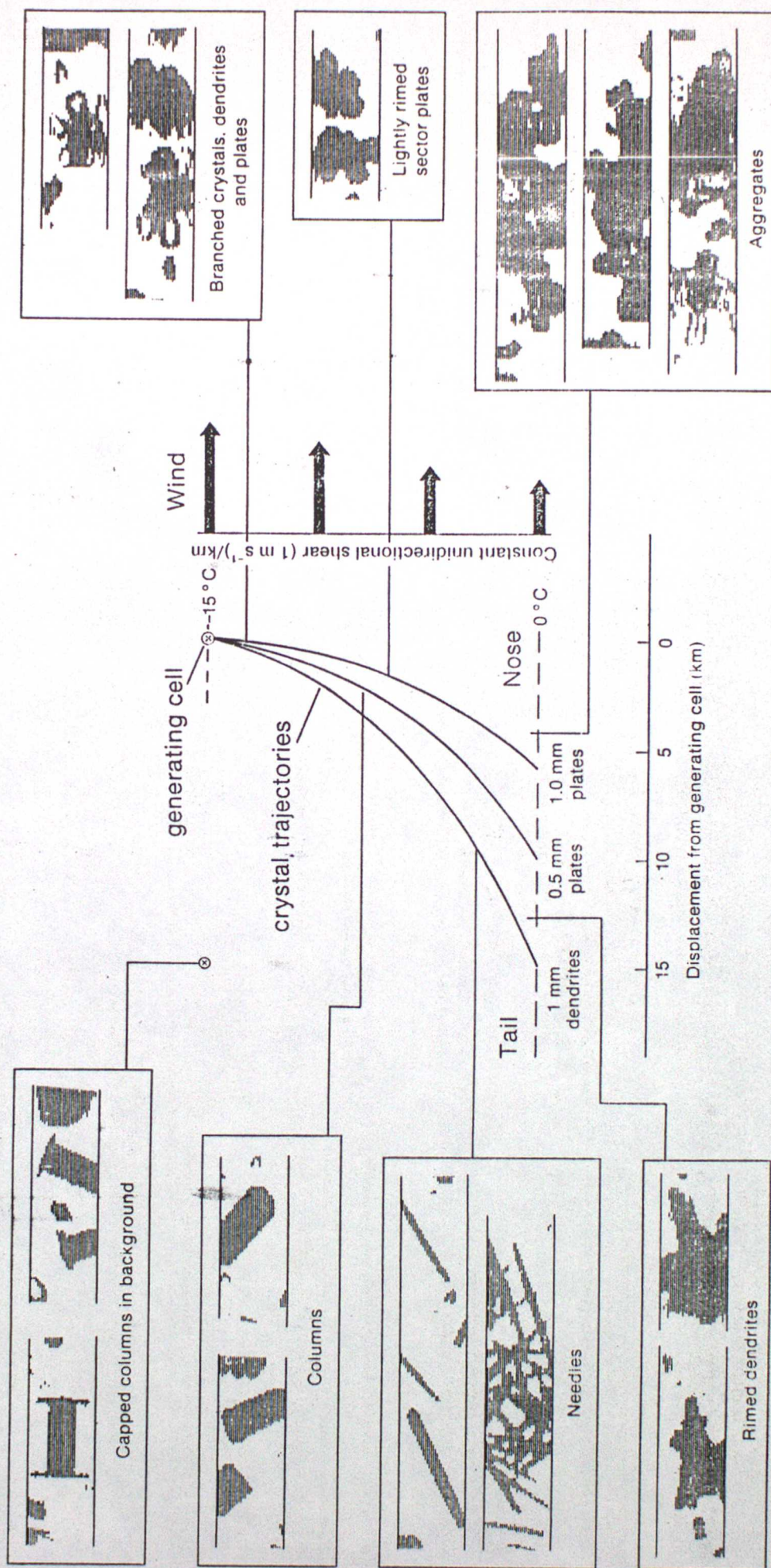
Rimed needles : 28 km



Mixed aggregates and platforms : 40 km







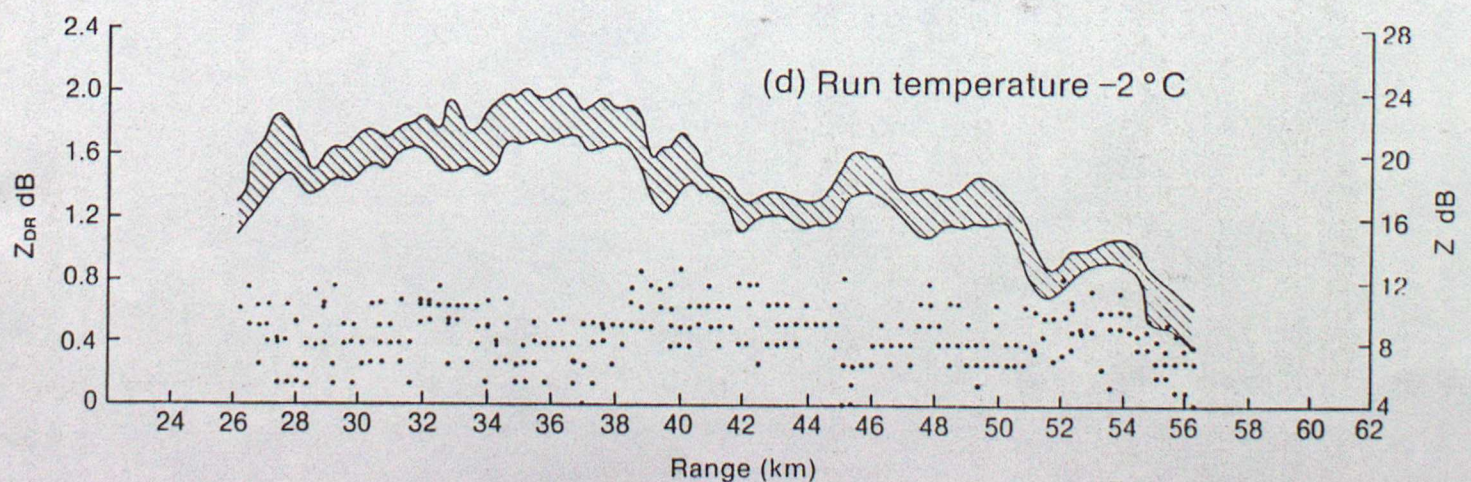
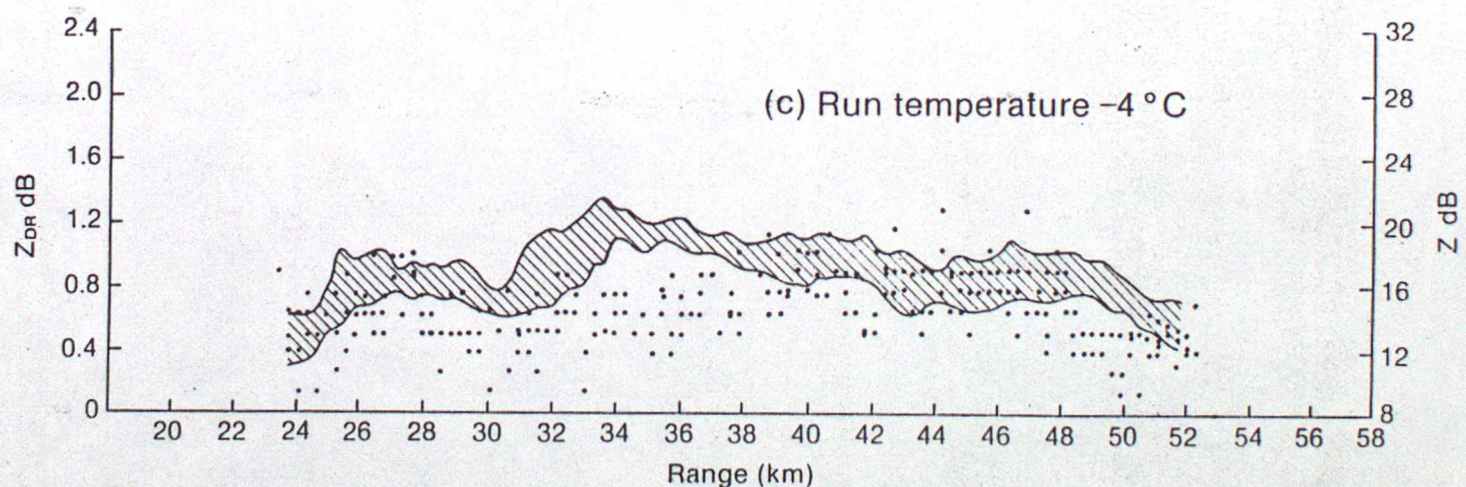
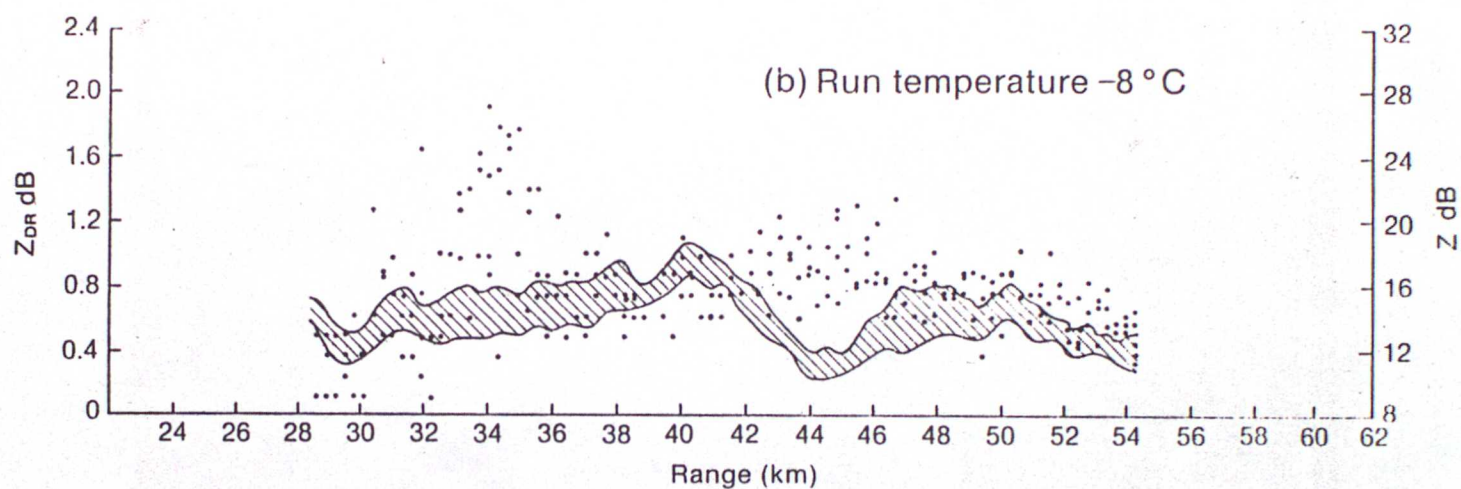
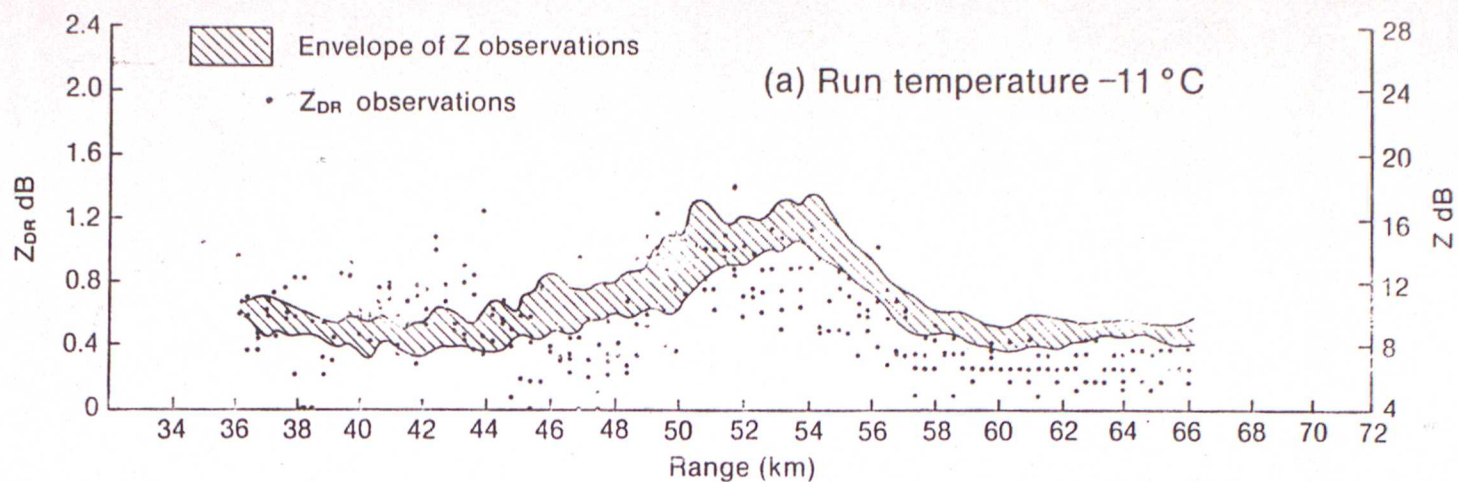


FIG 8

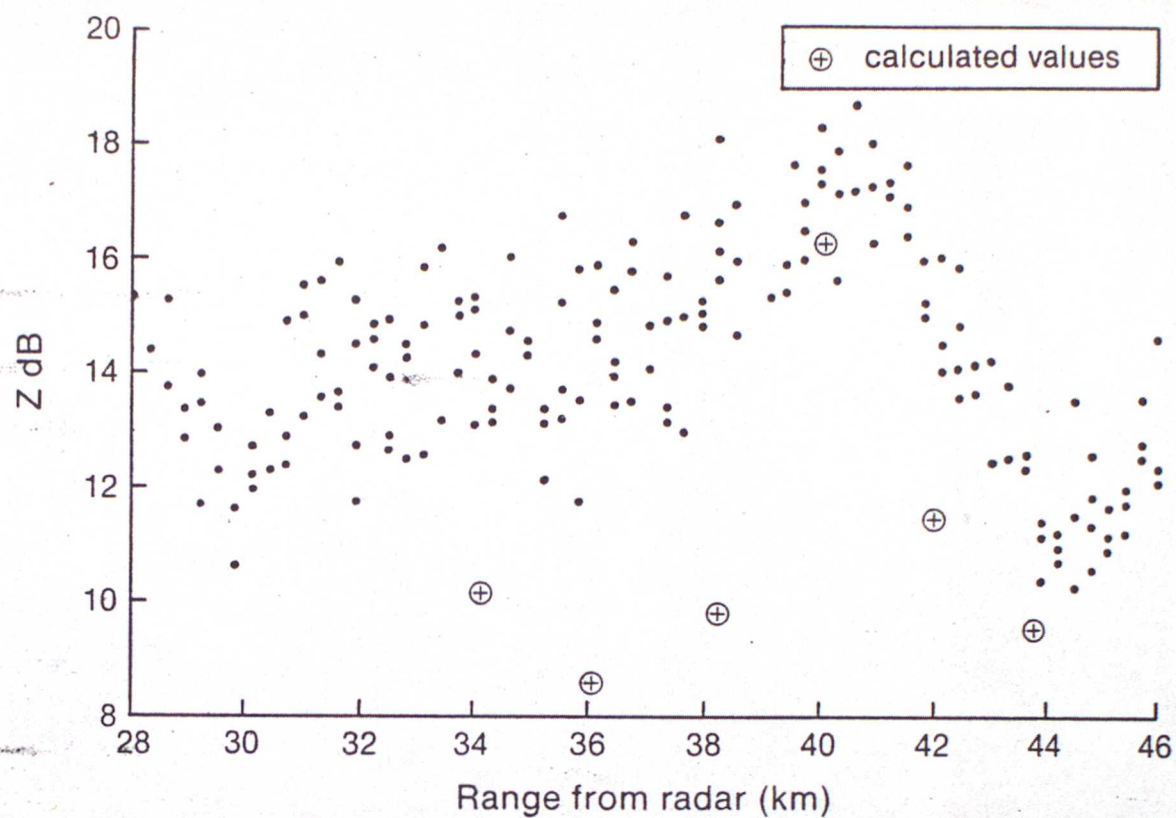


Fig. 9a

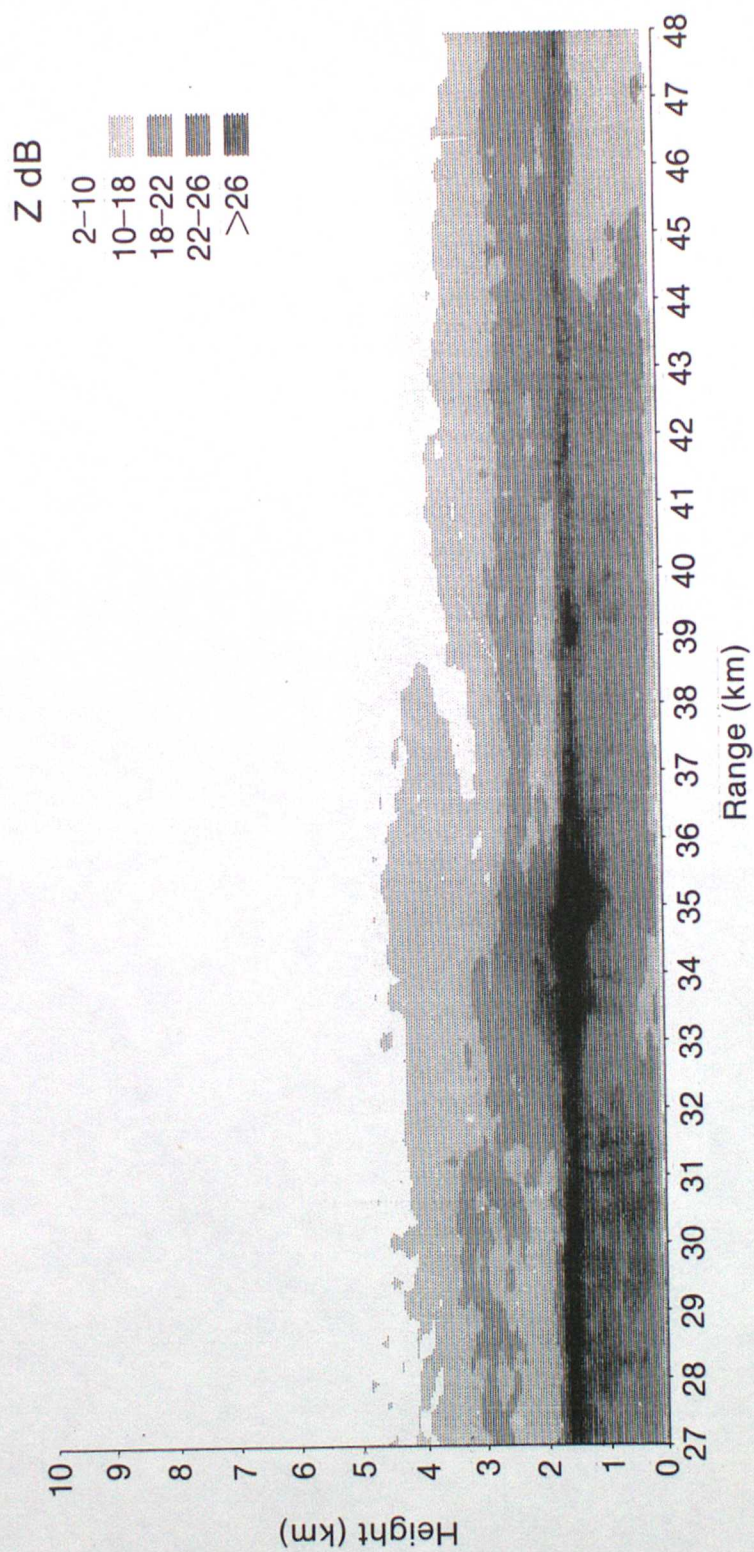
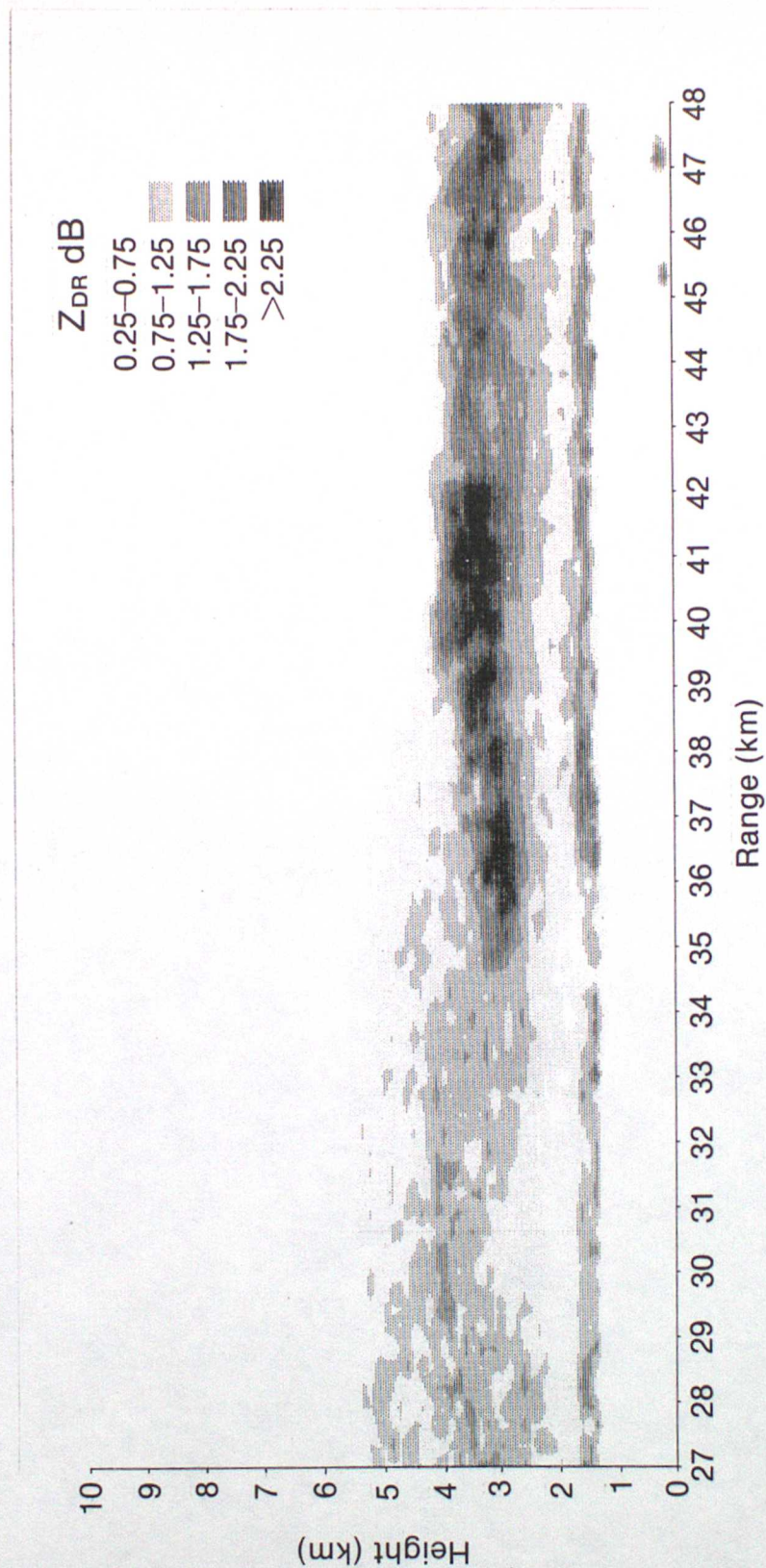
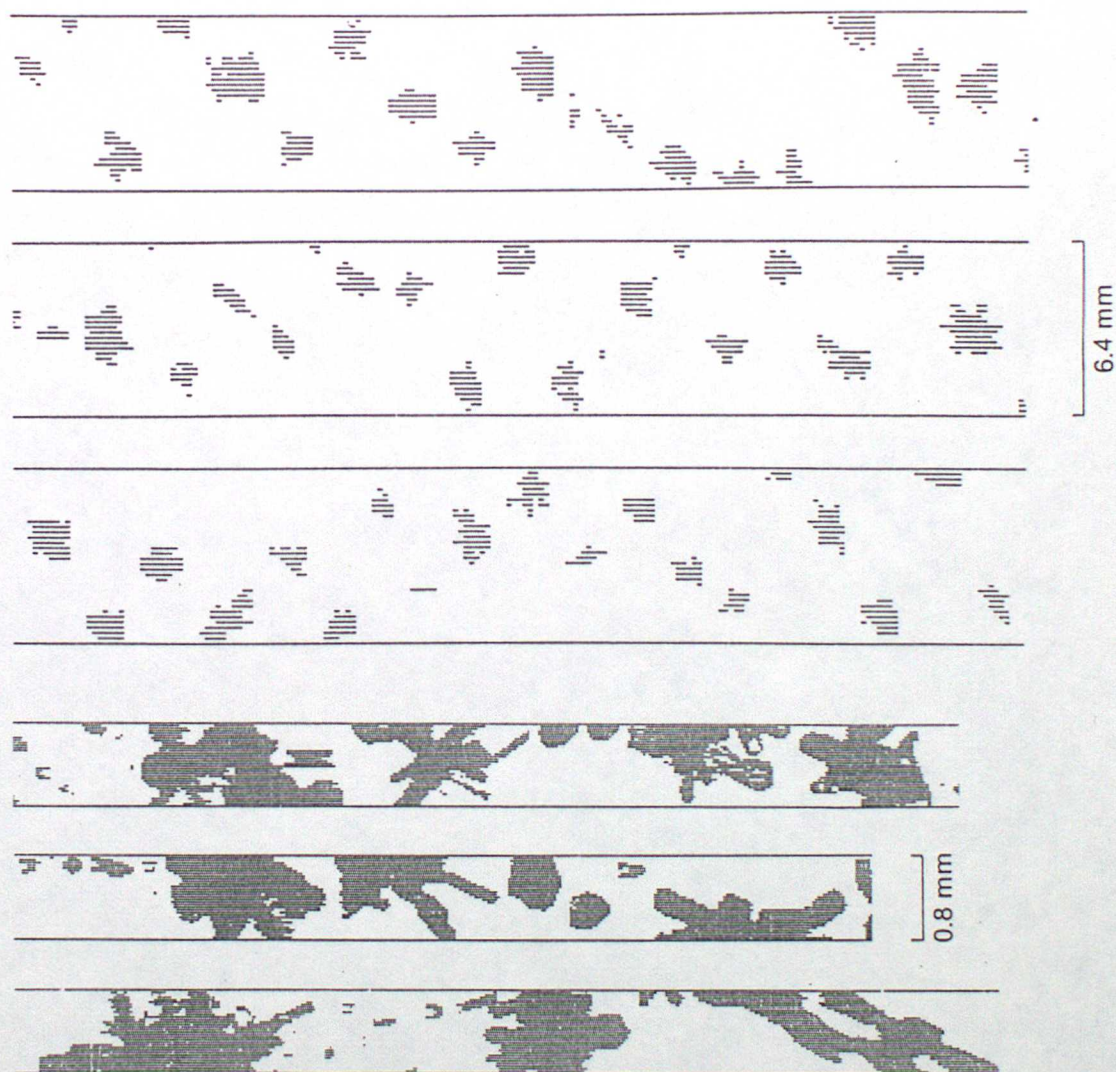


Fig 9.6



(a) Height 3.0 km (-7°C)

Range 37 km $Z_{\text{DR}} = 3.0 \text{ dB}$, $Z = 10 \text{ dB}$



(b) Height 3.0 km (-7°C)

Range 33 km $Z_{\text{DR}} = 1.0 \text{ dB}$, $Z = 19 \text{ dB}$

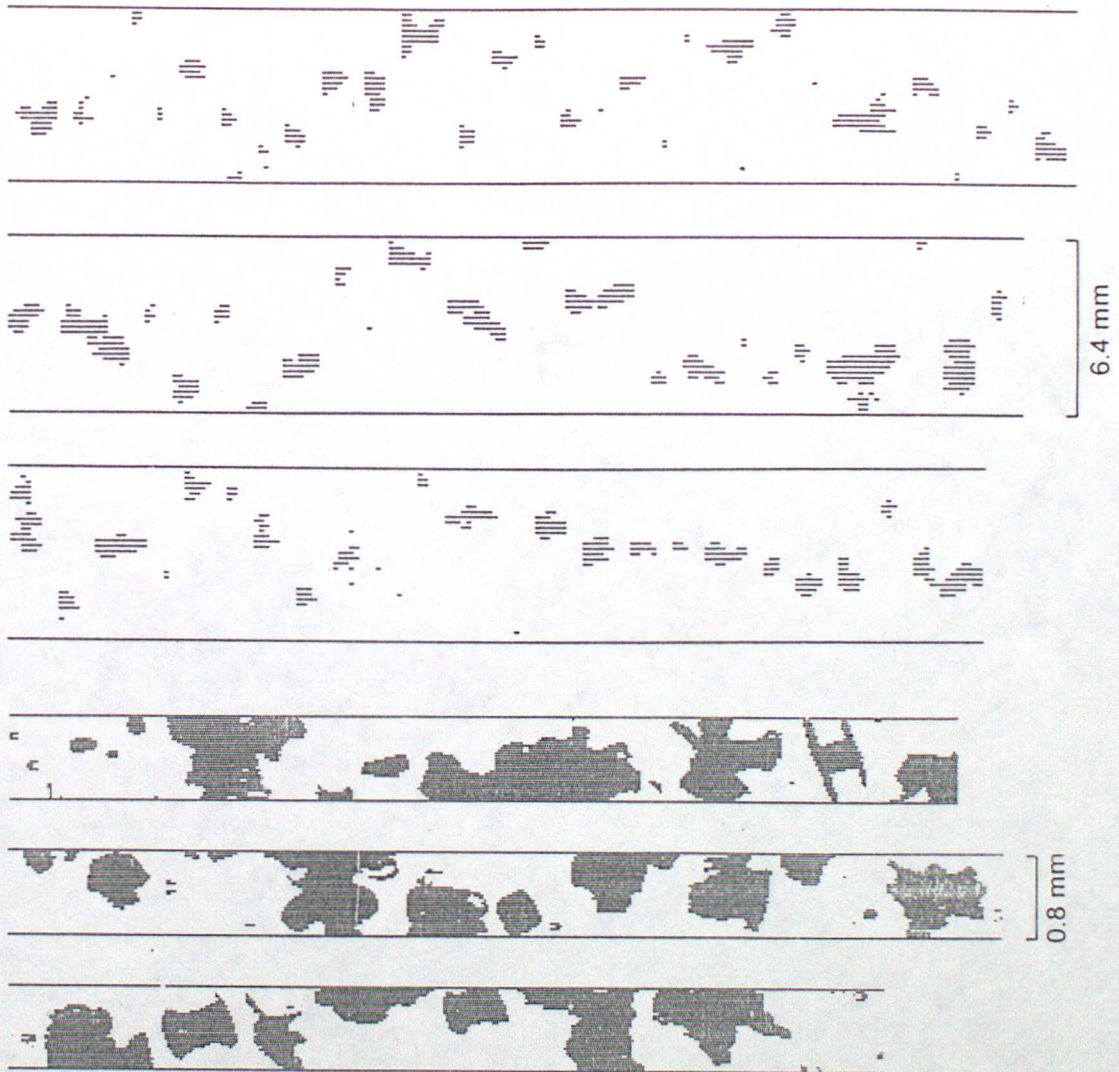
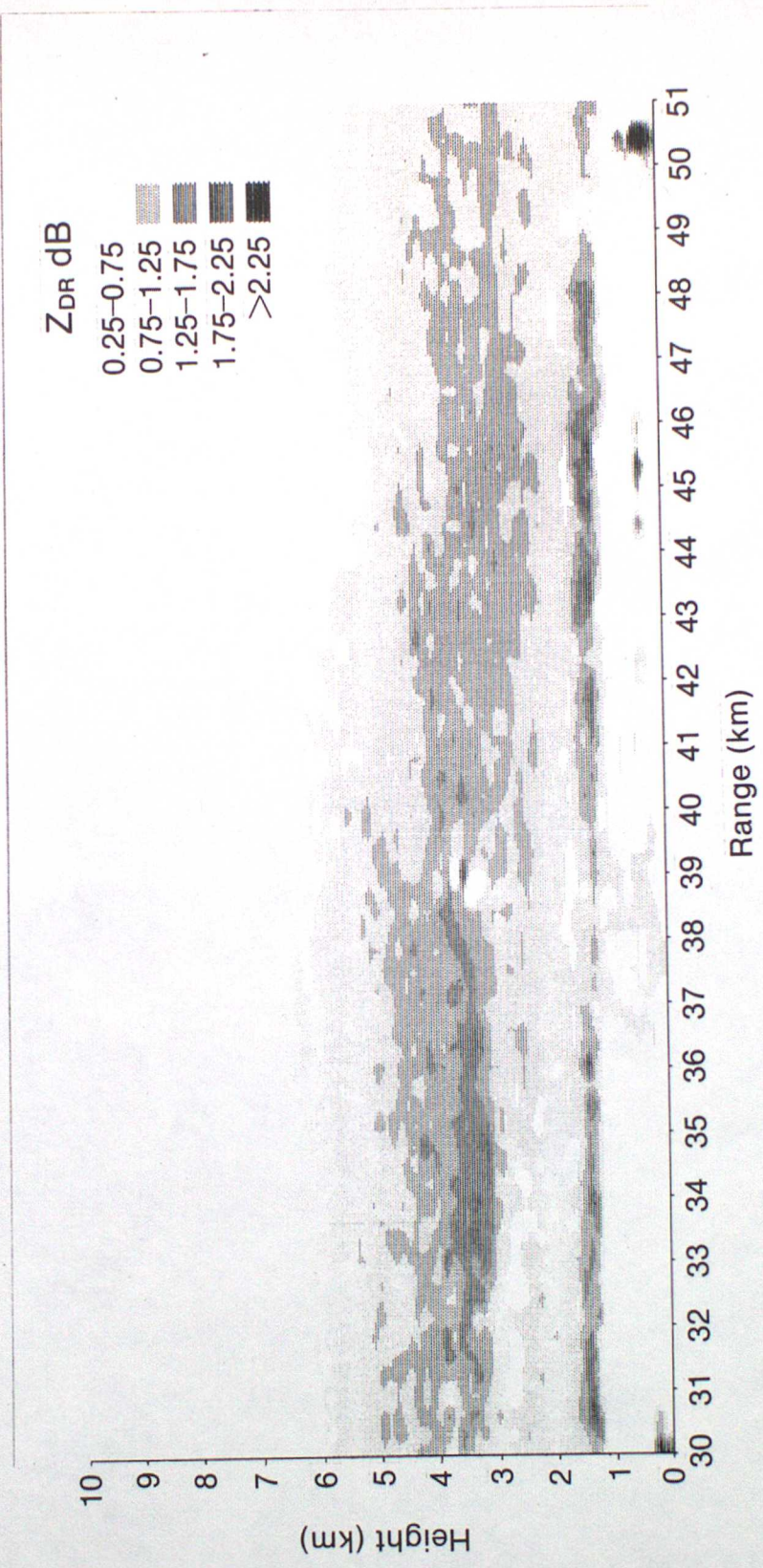


Fig 11a

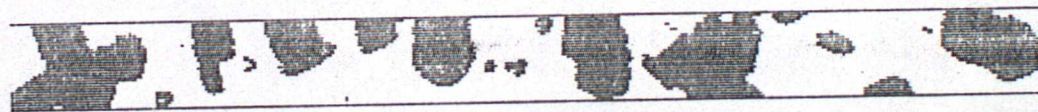


Fig 11.6

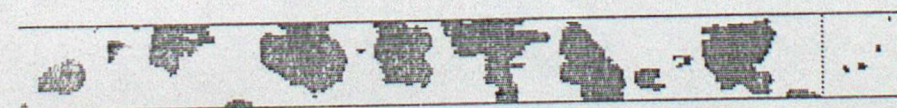
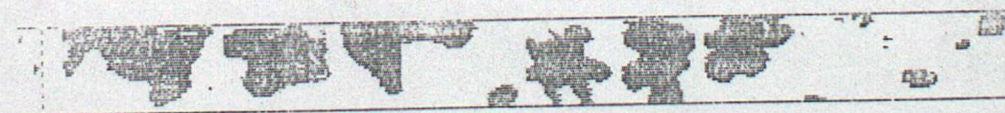


Height 3.1 km (-8°C)

Range 34 km $Z_{\text{DR}} = 1.9 \text{ dB}$, $Z = 14 \text{ dB}$



Range 40 km $Z_{\text{DR}} = 0.8 \text{ dB}$, $Z = 16 \text{ dB}$



0.8 mm

